Available online at www.sciencedirect.com

ScienceDirect

Solar Energy 103 (2014) 525–540

SOLAR ENERGY

www.elsevier.com/locate/solener

Performance analysis of a dielectric based 3D building integrated concentrating photovoltaic system

Hasan Baig [a], Nazmi Sellami [a], Daniel Chemisana [b], Joan Rosell [b], Tapas K. Mallick [a,*]

[a] *Environment and Sustainability Institute, University of Exeter, Penryn Campus, Penryn TR10 9FE, United Kingdom*
[b] *University of Lleida, Lleida, Spain*

Received 15 July 2013; received in revised form 20 December 2013; accepted 4 March 2014
Available online 24 March 2014

Communicated by: Associate Editor Jayanta Kumar Nayak

Abstract

The use of concentrating photovoltaic systems (CPV) in building integration has spurred towards the development of newer products, which have the potential to offer the convenience of pleasing architecture and day lighting along with simultaneous production of clean energy. This paper addresses the energy transformations and the expected energy output of a low concentrating photovoltaic system designed to have a geometric concentration of 3.6×. The optical element used is a three dimensional Cross Compound Concentrator (3DCCPC) made from clear polyurethane material. Small sized silicon solar cells based on the Laser Grooved Buried Contact (LGBC) technology having an absorber area of 1 cm^2 are utilised in the system. Both experimental and numerical analyses are performed confirming the optical, electrical and thermal performance of the system. While performing the optical analysis the concentrator was found to have a maximum optical efficiency of 73.4%. A maximum power ratio of 2.67 was observed when comparing the electrical output of the concentrator unit with a non-concentrating counterpart. The effects of non-uniformity caused by the use of the concentrator are analysed. The non-uniformity of flux distribution showed an average drop of 2.2% in the I_{sc} values which is again reflected in the overall power output. Manufacturing defects like the cell and concentrator misalignments are addressed and their impact on the overall performance are verified by numerical simulations. The operating temperature of the solar cells was found to have a parasitic effect on the overall performance of the system. A maximum temperature of 332 K was observed in the solar cell at 0° incidence and a incoming radiation of 1000 W/m^2 which brings down the overall power production by 14.6%. Finally, the expected system output over a given time period is presented showing the strengths and weakness while employing such a system.
© 2014 Elsevier Ltd. All rights reserved.

Keywords: 3DCCPC; Non-uniform; CPV; BiCPV; CPC

1. Introduction

The rising energy prices and climate change have spurred the renewable energy revolution across the globe, driving us towards self-sustaining energy resources and the technology to harness it. Solar energy has proven to be one such potential alternative energy resource, which can be used for meeting our energy demands. The energy from the sun can be directly converted into electricity by the use of photovoltaic (PV) technology. According to a report by the International Energy Agency (Lausten, 2008) buildings consume more than 40% of world's energy. The adoption of PV technology in residential applications has seen an increasing trend for its application in the last few years. Starting with simple PV panels the industry is now moving towards Building integrated photovoltaics

* Corresponding author. Tel.: +44 01326 259465.
E-mail addresses: mail2baig@gmail.com, t.k.mallick@exeter.ac.uk (T.K. Mallick).

http://dx.doi.org/10.1016/j.solener.2014.03.002
0038-092X/© 2014 Elsevier Ltd. All rights reserved.

(BIPV) systems. These systems are designed to integrate PV systems seamlessly into structural elements of the buildings, making them a functional part of the building architecture. Such systems include semi transparent facades (Park et al., 2010), glass ceilings (Hughes, 2009), clay solar tiles (Magazine, 2010), thin films (Yoon et al., 2011) and Sphelar® cells (Biancardo et al., 2007). A review of some of the notable solutions are presented under (Petter Jelle et al., 2012) addressing their satisfactory appearance and high efficiencies with good weather stability. These systems however have huge costs associated with them making them less feasible for general applications.

Concentrating sunlight and focusing it on smaller sized cells can be sought as a viable solution in reducing the use of expensive solar cell materials for niche application as building fenestrations. Further, integrating these systems in our existing building structural elements could prosper the technology and increase its usage. Such applications can be categorised as Building integrated concentrating photovoltaic (BICPV) systems, which can prove to be the right solution towards sustainable modern buildings. These applications will help in having an optimised day lighting and simultaneous energy production, bringing efficient buildings closer to reality. Using the principle of concentrating sunlight reduces the amount of solar cell material required and makes it more cost effective. Integrating the structural elements like windows, facades, sky lighting, cladding, curtain wall, etc. with concentrating photovoltaic technology further adds prospects of an entirely new market in its own. Only a few of such applications have been developed across the world over the last decade (Zacharopoulos et al., 2000) (Nilsson et al., 2007; Tripanagnostopoulos et al., 2007), some of the recent developments have been reviewed (Chemisana, 2011). Few other developments very recently undertaken by our research group can be found under (Baig et al., 2012a,b; Sarmah et al., 2011; Mammo et al., 2013; Sellami et al., 2012; Sellami et al., 2011a,b,c; Baig et al., 2013). A new concept of integrating concentrating photovoltaics has been recently demonstrated by (Mammo et al., 2013), where a reflective type three dimensional compound parabolic concentrator (3D CCPC PV) was used as the optical concentrating element. The system maximum power output was found to be three times that of the similar kind of non-concentrator system with maximum electrical conversion efficiency of 14%. A 3D static concentrator called the square elliptical hyperboloid (SEH) with 4× was presented recently (Sellami et al., 2011a,b,c), this system was built using dielectric material and worked on the concept of total internal reflection. The system was found to have an optical efficiency of 40% with a wider acceptance angle equalling 120° thus enabling the sunlight capture all day from both direct and diffuse radiations. A similar system but with variable heights is presented under (Sellami and Mallick, 2012) recently. A two dimensional linear asymmetric CPC system based on dielectric concentrator was analysed by (Sarmah et al., 2011; Baig et al., 2013) the system has a concentration ratio of 2.8 capable of having maximum power ratios of 2.27. A system based on see-through prism CPV module for window integrated photovoltaics was analysed by (Yamada et al., 2011). This system generates approximately 1.15 times more electricity than a conventional module while operating with 63% less solar cell area. Other systems based on CPV/T concepts having a CR > 2.5× were addressed by (Tripanagnostopoulos et al., 2009) in which the thermal and PV module work together or separately with and without tracking mechanisms.

The current study brings forward a dielectric based three dimensional cross compound CPC (3DCCPC) with square entry and exit aperture. Earlier work on a reflecting type 3DCCPC may be found under (Mammo et al., 2013). This work introduces a refractive system using similar design features. The three dimensional shape is attained by sweeping the 2DCPC over a square profile. In this work, a refractive based prototype of the system is designed, manufactured and analysed both experimentally and numerically. Use of ray trace method is made to carry out the optical analysis of the concentrating element and finite element methods are applied to carry out the electrical and thermal analysis of the system. Results obtained are validated experimentally and the gaps highlighted.

2. System description

The system under study essentially consists of a concentrator element, an encapsulation material and a solar cell essentially placed between two glass sheets.

2.1. Concentrator

The concept of the compound parabolic concentrator (CPC) has been utilised in numerous solar energy applications including both thermal and photovoltaics. The concentrator element used in our study is a dielectric material based Three Dimensional Cross Compound Parabolic Concentrator (3DCCPC). The three dimensional design allows light to be concentrated in all the directions via total internal reflection. The concentrator geometry was designed by simply sweeping a segment of parabola about a square cross section as shown in Fig. 1. The details on the equations of the parabolic segment of the CPC can be found under (Sellami and Mallick, 2013) and (O'Gallagher, 2008). The refraction on its front air and dielectric interface allows having better external acceptance angle. The system is desired to have a concentration ratio (C) of 4×, using the following equation:

$$C = \left[\frac{n_R}{\mathrm{Sin}(\theta_a)}\right]^2 \tag{1}$$

The system half acceptance angle (θ_a) is found to be 48.5° for a refractive index (n_R) of 1.5, entry side of 20 mm and a height of 25.9 mm. However this is truncated by almost 37.6% to get a truncated height of 16.16 mm and

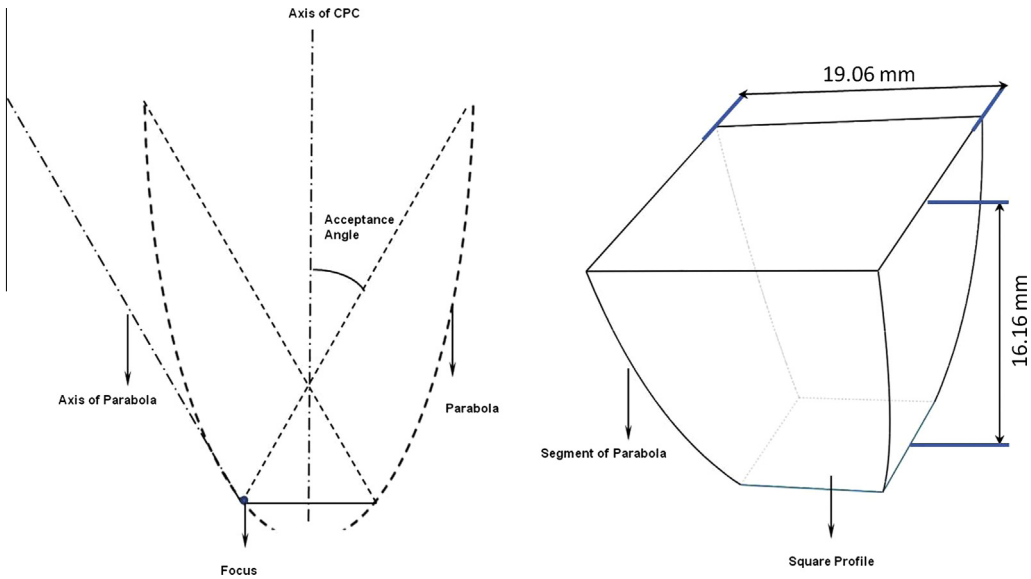

Fig. 1. Schematic design of the 3DCCPC.

a concentration ratio of 3.6× with entry and exit aperture sides of 19 mm and 10 mm respectively as shown in Fig. 1. The truncation would also impact on the acceptance angle which can be seen while performing the optical analysis in later sections. The concentrator used in our study as shown in Fig. 2 was made using a polyurethane material crystal-clear 200® (http://www.smooth-on.com/tb/files/CRYSTAL_CLEAR_200_TB.pdf).

One of its main features is that it is transparent and refracts all the light entering the aperture via total internal reflection. The refractive index of the material is shown in Fig. 3. It has good transmission properties and excellent strength and rigidity to retain the shape of the complex profile.

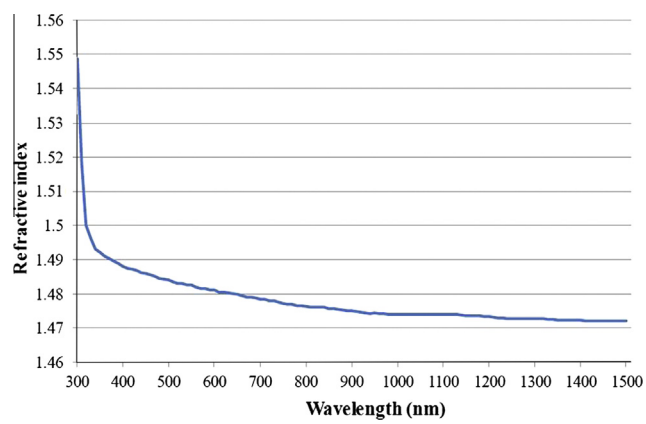

Fig. 3. Refractive index of Polyurethane.

2.2. Solar cell

The solar cell used in the system and its design is shown in Fig. 4. The solar cell used in this study is based on the Laser Grooved Buried Contact (LGBC) technology (Heasman et al., 2007) but any other advanced solar cell technology may be utilised while using the same concentrating element. The silicon solar cell used in the present study has 13 fingers each 35 μm wide and a bus bar of width 1 mm. These cells have been optimised to perform under conditions upto 10×, hence are utilised in this system. A small visual difference between the designed solar cell and the cell used in analysis, which basically occurs in laser cutting of the cells in huge quantities, however it has negligible effect on the overall performance.

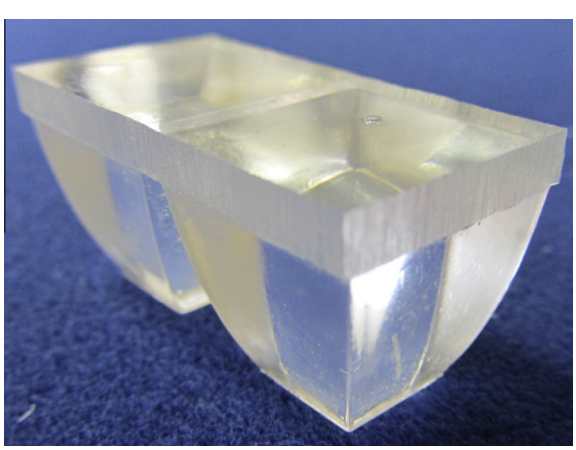

Fig. 2. Sample of the concentrator element made using polyurethane.

2.3. Encapsulation material

The purpose of using an encapsulation material is to increase the lifetime of the solar cell while protecting it from the moisture. Good transmission properties are always desired from an encapsulant to be used in building integration. The use of Sylgaurd-184 (Anon, 2008) as an encapsulation material is made in our system. The

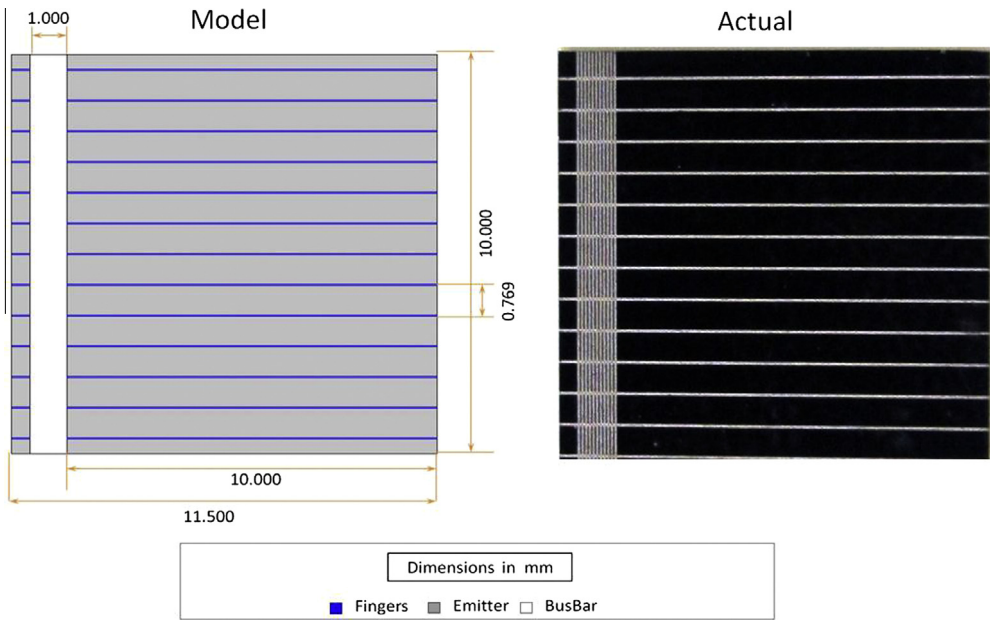

Fig. 4. Solar Cell geometry used in the numerical and the experimental analysis.

encapsulant plays a dual role; firstly it acts as an adhesive and helps in holding the concentrator to the solar cell, secondly it functions as a perfect encapsulation material and protects the solar cell from weathering.

2.4. Assembly

Initially the concentrator units are casted using the polyurethane material, they are later cured at room temperature to obtain series of concentrator units as shown in Fig. 2. The solar cells are soldered using thin tin plated copper strips and suitable series or parallel strings are prepared. The cells are then placed on a glass plate and fixed using a glue material. The encapsulant is then prepared and poured all over the solar cells and distributed smoothly over the surface. Later the concentrator is placed over the solar cells and the system is left to dry overnight. One of the limitations during this process is that small misalignment occurs between the solar cell and the concentrator which can cause optical losses. A typical prototype employing 9 such units is shown in Fig. 5. The three rows are connected in parallel with each row having three cells in series.

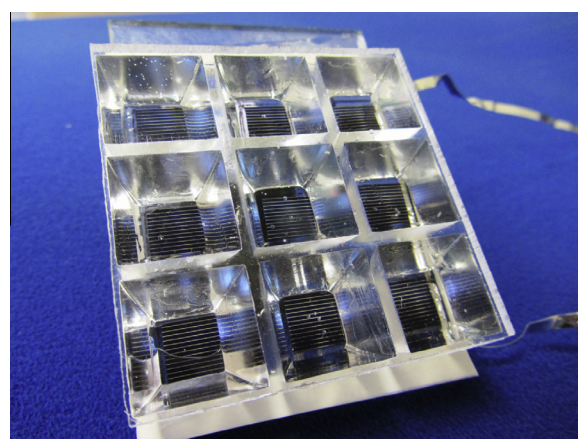

Fig. 5. Sample system with nine CCPC units.

3. Optical analysis and performance

The optical power output while using a concentrator unit can be obtained by carrying out ray trace analysis of the system. In the present study a ray trace simulation software OptisWorks (Sellami, 2011) was used to carry out the optical analysis. In the ray trace method, the rays entering the concentrator are assumed to be parallel and refract depending on the refractive index of the material. The simulations were carried out for polyurethane based 3DCCPC at AM 1.5D, the system was evaluated without a glass cover by varying the angles of incidence in longitudinal direction between 0° and 90°. The absorptance of the polymer material used in making the concentrator as a function of the incoming solar radiation used in the study in shown in Fig. 6. It may be seen that there exists minimal absorption over the wavelength range of 350–1100 nm.

The optical model was based on the refraction laws where a source of light with desired intensity is focused on the concentrator and the output along the absorber surface is estimated. The optical efficiency of the CPC is obtained for different incident angles of the incident rays. For each incident angle, an optical simulation is carried out determining the energy of the incident rays reaching the solar cells after going through the refractive element. Fig. 7 shows an illustration of the concentrated incident rays having a range of incident angles (−15°, 0°, 25°, 34.5° and 50°) to the normal of the CPC entry aperture to highlight the different behaviour inside the optical

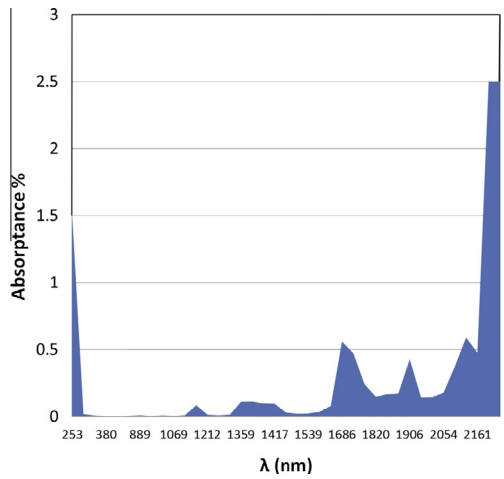

Fig. 6. Absorptance of polyurethane.

concentrating element. The figure represents how the rays reach the base of the system in a non-uniform fashion causing hotspots at particular areas of the solar cell. A small portion of the rays can also be seen bouncing back or escaping out through the concentrator depending on their entry. The rays escaping could be of help in illuminating the space behind helping in regulating the sunlight when used as a building integrating system. Fig. 8 shows the variation of the optical efficiency with respect to the incidence angle. The use of refractive material provided a higher acceptance angle in the initial design which was about 48.5°, however, the amount of refractive material required was very high and was truncated due to which the overall acceptance angle increases to about 70° as shown in Fig. 8. Based on the optical efficiency obtained another plot for the percentage of transmission vs. the incidence angle is plotted assuming a 100% transmission at 0°. It may be seen that for all angles less than 34.5° more than 90% light entering the concentrator reaches the absorber as can be seen in Fig. 8. It may also be noted that these results represents both the E–W and N–S ray trace outputs. The system has a greater acceptance angle but lower optical efficiency as compared to the reflective system with a similar geometry studied recently (Sellami and Mallick, 2013).

The square geometry also provides a cost benefit as the solar cells are mostly available in square or rectangular shapes, having them in circular or elliptical shape would increase the cost of the solar cell per unit area. The spacing between the optical concentrator may be utilised for optimising the day lighting through the system.

The performance of the photovoltaic concentrator can be experimentally analysed by evaluating the performance of a CPV module with the concentrator and comparing it with a non-concentrating counterpart. In an indoor controlled environment the module can be analysed for particular radiation intensity with different incident angles. For a static dielectric concentrator designed for a particular range of acceptance angles, it is very important to evaluate the performance for all the incidence angles within the range. While carrying out the optical analysis by ray trace method an illuminance detector is placed at the exit of the concentrator. The detector gives the flux distribution and energy of the concentrated rays by the concentrator. The detector is defined to be the exact size of the exit aperture of the concentrator and characterised to measure only the illumination coming from the concentrator. The optical performance of the system has also been analysed experimentally (Sellami, 2011) and by simulation at every 10° interval to determine its optical performance whose results are shown in Fig. 9.

The rays exiting the concentrator element are found to have a non-uniform distribution along the solar cell. This non-uniformity plays an important role in the performance of the system (Baig et al., 2012a,b). It may be seen in Fig. 10 how the illumination intensity varies along the cell spatially at different angles of incidence. The highest intensity along the solar cell may exceed up to 20 suns as can be seen in the case of incidence angle 20°, i.e. for the case of angles below the acceptance angle and can fall to values even lower than the concentration ratio as can be seen in the case of 60° incident angle, i.e. for cases of incident angle higher than the acceptance angles. These phenomena were not addressed in the earlier studies mostly because simple five parameter models were utilised to evaluate the average power output of the system. However, we have now used the finite element method to analyse the impact numerically

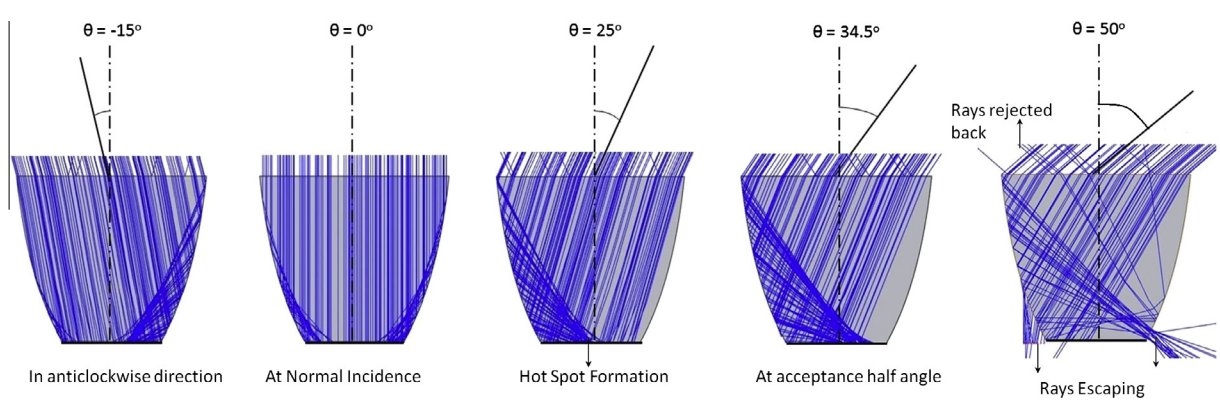

Fig. 7. Ray tracing diagrams of the CPC for −15°, 0°, 25°, 34.5° and 50° incidence angle.

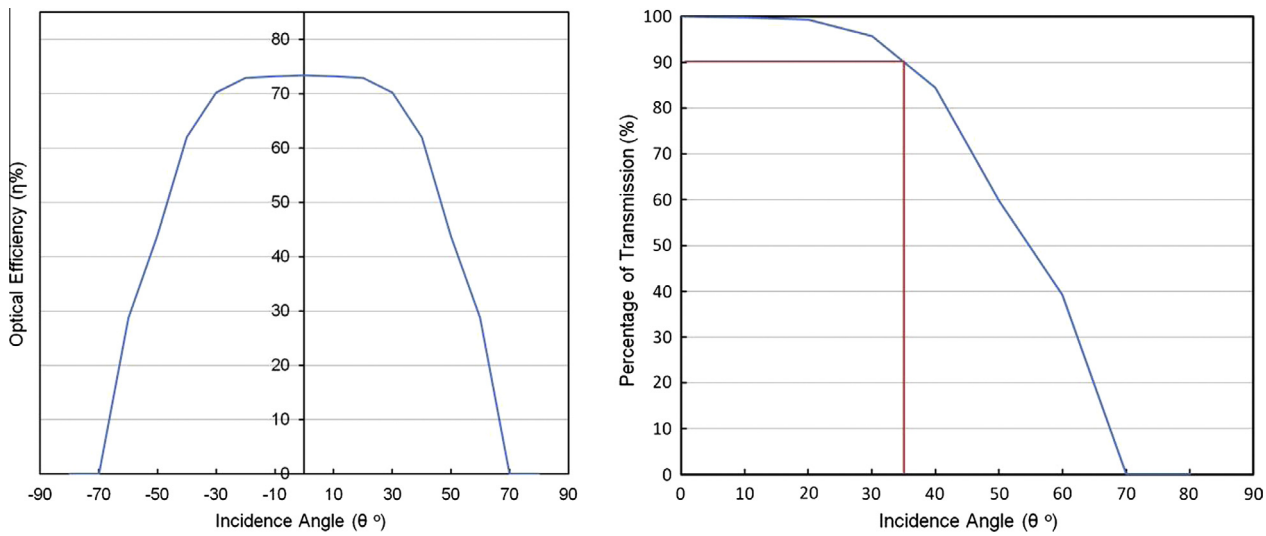

Fig. 8. Variation of optical efficiency and transmission percentage with incidence angle under direct solar radiation.

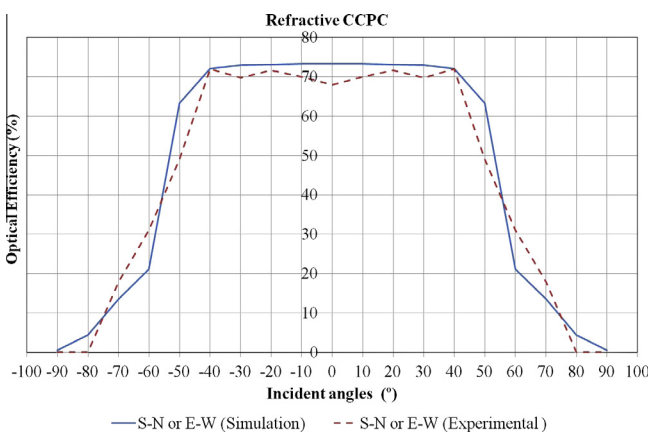

Fig. 9. Comparison between the experimental and calculated optical performance.

and validate its effects experimentally in the present study. The output illumination intensity distribution as shown in Fig. 10 is utilised to determine the electrical performance of the system.

The non-uniformity of the illumination is a complex property and may be expressed in several forms. In the case of the concentrating system, the non-uniformity on the solar cell varies with its location, at some points the flux may be highly non-uniform and at some points it might be completely uniform. In order to quantify this term as a general number is not correct, since several different illumination distributions may give the same mathematical result, but would represent different physical distributions. However, in order to explore this effect it's important to perform some mathematical way to express the non-uniformity. A spatial non uniformity factor (α) was proposed recently by (Lu et al., 2009) and has been utilised here to define the extent and effect of non-uniformity in the illumination, neglecting its quality. The spatial non uniformity factor (α) is defined as the ratio of the difference of the maximum and minimum incident flux to their sum as shown in the following equation:

$$\alpha = \frac{G_{\max} - G_{\min}}{G_{\max} + G_{\min}} \tag{2}$$

where $G_{\max}$ and $G_{\min}$ indicate the highest and the lowest flux along the solar cell surface whose values are tabulated in Table 1. The non-uniformity parameter is analysed at different incident angles, as shown in Fig. 11.

From Table 1 it may be clearly seen that a very high non-uniformity in the incident flux exists in the system. Higher values of ranging around 20 suns may be observed at angles of incidence ranging between 20° and 40°. It may also be noted that the average illumination reduces significantly, once the incident angle crosses the acceptance angle. The impact of the non-uniformity on the overall performance of the system is not simple to be accessed, since a series of factors come under play while determining the impact (Baig et al., 2012a,b). The non-uniformity can be found at every incidence angle, hence making it important to include the flux distribution over the solar cell surface instead of using an average value of the illumination intensity. This illumination intensity has been utilised to carry out the electrical and thermal analysis as shown in the following sections.

4. Electrical analysis and performance

The solar cell can be modelled using either the one diode or the two diode equation as shown in Fig. 12. In the present study both models were tested for their accuracy and one-dimensional model was selected. The term I_D represents the diode current and the term I_{ph} represents the photo-generated current. The total current flowing in the external load R_L is given by Eqs. (3) and (4) respectively. The term I_0 represents the reverse saturation diode current corresponding to the diffusion and recombination of electrons and holes in the p and n sides of the cell, V is

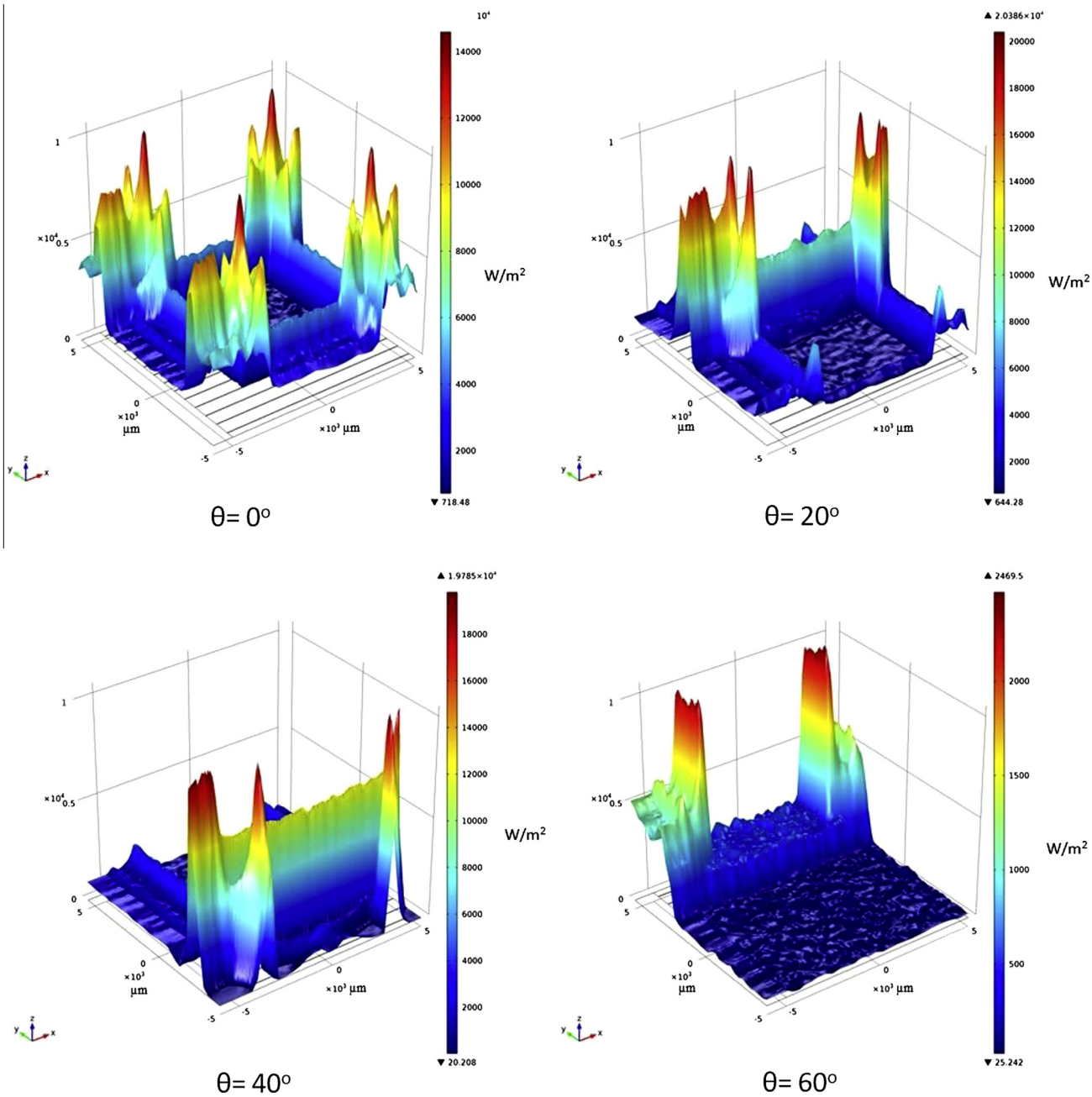

Fig. 10. Flux distribution on the solar cell.

the mean cell voltage across the external load resistance R_L and V_T is the thermodynamic voltage, V_j is the junction potential, k_B is the Boltzmann constant, q is the electron charge and n is the ideality factor which is usually greater than 1.

$$I = I_{ph} - I_D \tag{3}$$

$$I = I_{ph} - I_0\left[\exp\left[\frac{V_j}{nV_T}\right] - 1\right] - \frac{V_j}{R_{sh}} \tag{4}$$

$$V_T = k_B T/q_e \tag{5}$$

$$V_j = V + IR_s \tag{6}$$

Eq. (4) is the general form of current generated in a solar cell; it may further be reduced depending on the emitter region I_e and the dark or finger region I_{da}. The term I_{ph} strongly depends on the illumination and is directly proportional to its intensity.

$$I_e = I_{ph} - I_0\left[\exp\left[\frac{V_j}{nV_T}\right] - 1\right] - \frac{V_j}{R_{sh}} \tag{7}$$

$$I_d a = I_0\left[\exp\left[\frac{V_j}{nV_T}\right] - 1\right] - \frac{V_j}{R_{sh}} \tag{8}$$

The incident solar radiation leads to the increase of the temperature of the solar cell which further increases the population of electrons exponentially enhancing the dark saturation current. The dependence of the saturation current on the temperature (Rosell and Ibáñez, 2006) is

Table 1
Variation of non uniformity parameter α with incident angle θ.

Incident angle (θ)	Illumination intensity G(W/m^2)			Non uniformity (α)
	Max	Min	Avg	
0	14767.5	717.6	2997.8	0.907
10	18733.8	698.1	2942.7	0.928
20	20573.6	642.5	2796.4	0.939
30	22347.5	2.9	2548.8	0.999
40	19855.5	19.9	1984	0.998
50	3333.3	42.8	550.6	0.974
60	2496.6	24.6	272.8	0.98
70	1471.3	0	62.4	1
80	150.4	0	2.9	1
90	5.12	0	0	1

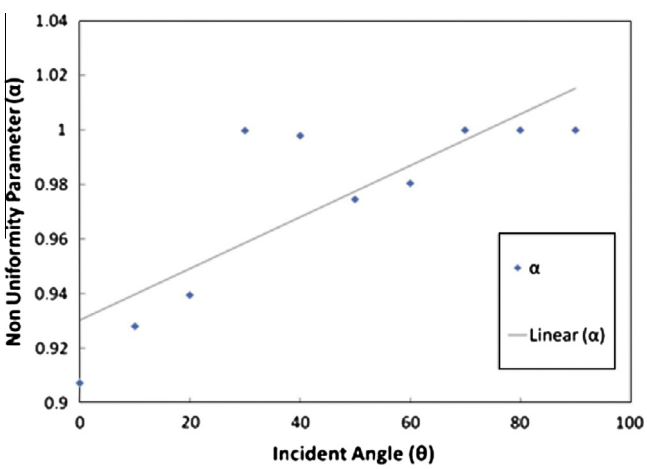

Fig. 11. Variation of spatial non-uniformity factor with incidence angle.

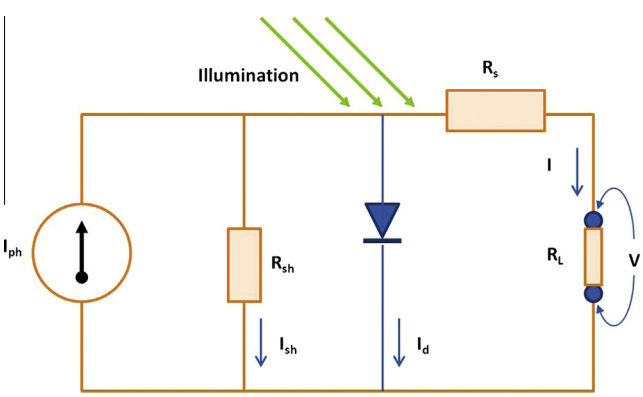

Fig. 12. Equivalent circuit of solar cell with one diode.

represented by Eq. (9) which suggests that its value increases with temperature but decrease with increasing material quality.

$$I_0(T) = I_{oo}T^3 \exp\left[\frac{-E_{go}}{k_B T}\right] \tag{9}$$

The terms I_{oo} and E_{go} represent the saturation current and the band gap energy at 0 K and are both approximately constant with respect to temperature. Employing the analogy expressed in (Chemisana, 2011) the equations may be represented in terms of generated current density (Q) as:

$$Q = j_1 G + j_2 T^3 \exp\left[\frac{-E_g}{k_B T}\right]\left(\exp\left[\frac{V_j}{nV_T}\right] - 1\right) + j_3 V_j \tag{10}$$

In order to solve the case with non-uniform illumination and determine the effective current density distribution on the surface, the solar cell needs to be simulated by solving the continuity equation as shown in Eq. (11). The continuity equation may be solved using finite element method. In our study finite element method is applied to obtain the solution using COMSOL Multiphysics software (Chemisana and Rosell, 2013). The governing equation solved over the solar cell domain is represented in the following equation:

$$-\nabla \cdot (\sigma \nabla V - J^e) = Q \tag{11}$$

where V is the electric potential, J^e is the current density and Q represents the current generated or the source term and σ is the conductivity of the material. The current generated in the illuminated emitter region Q_e and in the dark region Q_d may be expressed as:

$$Q_e = j_1 G + j_2 T^3 \exp\left[\frac{-E_g}{k_B T}\right]\left(\exp\left[\frac{V_j}{nV_T}\right] - 1\right) + j_3 V_j \tag{12}$$

$$Q_d = j_2 T^3 \exp\left[\frac{-E_g}{k_B T}\right]\left(\exp\left[\frac{V_j}{nV_T}\right] - 1\right) + j_3 V_j \tag{13}$$

Usually an I–V curve is used to demonstrate the performance of the solar cell and can be generated by superposition of the solar cell diode I–V curve in the dark with the light-generated current. The important parameters used to characterise the solar cell include the open circuit voltage (V_{oc}) also referred as zero current condition, short circuit current (I_{sc}) referred as zero voltage condition, and fill factor FF. Under a particular operating illumination condition the power (P) will be maximised at a point known as maximum power point. The parameter fill factor or 'FF' is defined as the ratio of the maximum power from the solar cell to the product of V_{oc} and I_{sc}.

The I–V curve is usually modelled under standard uniform illumination conditions, the presence of non uniformity and modification in the flux intensity (G) by concentration changes all the parameters and a modified I–V curve could be expected. The photovoltaic efficiency may be defined as shown in Eq. (14). Where the product G^*A is the power incident on the solar cell with area (A), and can be obtained using ray tracing techniques.

$$\eta = \frac{I_{sc} V_{oc} FF}{GA} \tag{14}$$

4.1. Solar cell parameters extraction and model validation

In order to validate our model and compare the numerical solution, I–V characteristics of the cell were evaluated under different uniform illumination intensities

and temperature to extract the constants j_1, j_2 and j_3 to be used in modelling. These constants have been fitted using statistical techniques over a range of different operating conditions of solar radiation and temperature whose results are shown in Fig. 13. Previous work has been carried out to show the constants obtained using a one diode model (Rosell and Ibáñez, 2006). In the present study, the experimental data for the solar cell were obtained using an indoor sun simulator at the Research Centre in Applied Energy, University of Lleida. It consists of a continuous light source concentrator device yielding 5000 W/m^2 irradiance. The PV cell was attached mechanically to the heat sink, ensuring a good electrical contact. A voltage was applied to the terminals of the PV cell using a bipolar power KepcoW source, model BOP 50-2M (Kepco, Inc., Flushing, NY). The cell voltage was measured by measuring the voltage drop over a calibrated resistance connected in series to the PV cell and KepcoW source. Data acquisition was made using a 16-bit analog-to digital converter, Campbell W CR23X (Campbell Scientific, Inc., Logan, UT). The fitted parameters j_1, j_2 and j_3 are further utilised to carry out finite element modelling. To confirm the accuracy of the model results all the measured current values are plotted against the simulated current values is shown in Fig. 14. The correlation ($I_{sim} = I^*_{exp}0.99$) and the coefficient of determination $R^2 = 0.99$ for the experimental and simulated currents indicates a good accuracy.

The parameters obtained and used are listed below in Table 2.

4.2. Electrical performance and validation of results

The electrical performance (I–V characteristics) of the solar cell was analysed using finite element modelling at different operating conditions. An example of such analysis is compared with the experimental results and is shown in Fig. 15.

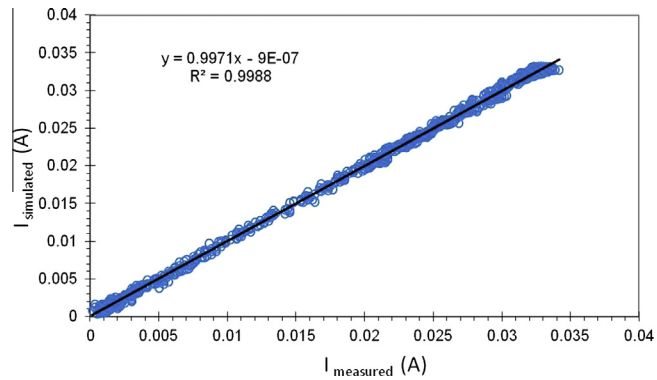

Fig. 14. Simulated vs. measured cell current for all the conditions.

It was reported earlier (Sellami, 2011) that there exist differences between the simulated and experimentally calculated optical efficiency whose values ranges within a value of about ±10%. The possible causes for this difference could be several factors. Some of the important factors could be the differences between the modelled and the actually manufactured concentrator surface qualities, geometry, moulding defects and absorption quality. Other factors include the misalignment of the solar cell caused during the manufacturing process and the spreading of the encapsulant layer around the borders of the concentrator causing the rays near the borders to escape out because of similar refractive index as shown in Fig. 16.

Fig. 17 shows the schematic setup used to carry out the experiments. The setup includes an ABET class-A solar simulator (Anon, 2009). The simulator consists of a xenon lamp and a filter to provide an AM1.5 solar spectrum. The

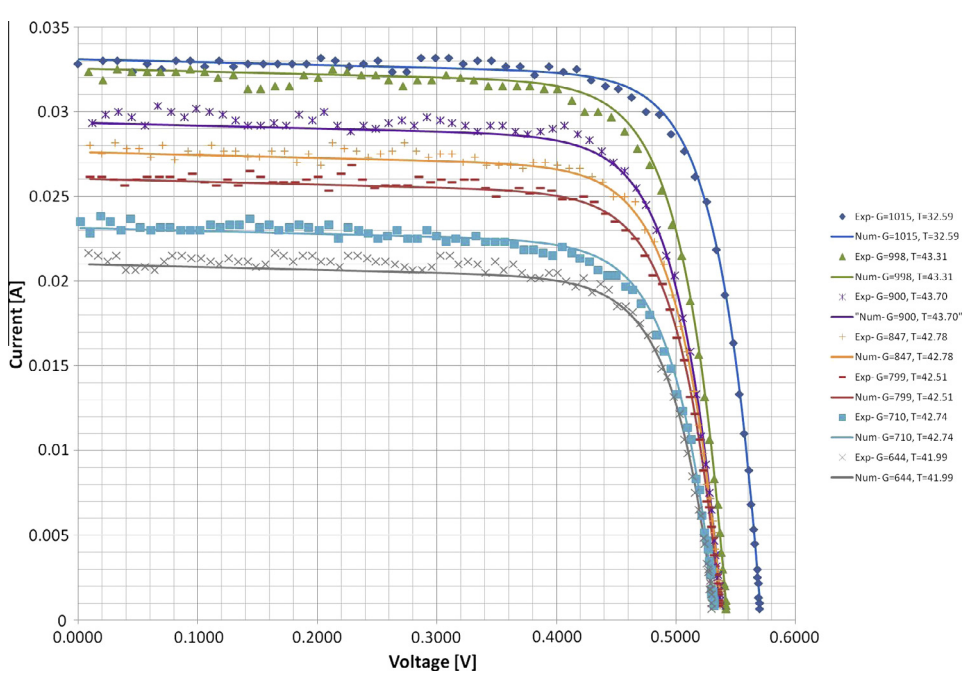

Fig. 13. Comparison of model simulated and experimentally obtained I–V characteristics for different levels of solar radiation and operating temperature.

Table 2
Solar cell parameters.

Cell parameters	Values
Cell width	11.5 mm
Cell length	10.0 mm
Busbar width	1.0 mm
Finger width	35 μm
Emitter sheet resistance	100 Ω/□
Finger resistance per unit length	0.3 Ω/cm
Operating conditions	
Illumination intensity range G	640–1015 W/m^2
Temperature range T	305–317 K
Diode equation parameters	
Constant j_1	0.32788 AW^{-1}
Constant j_2	−183824.4 Am^{-2} K^{-3}
Constant j_3	−20.578 Am^{-2} V^{-1}
Ideality factor n	1.13
E_g	1.124 eV
k_B	1.380×10^{-23} J K^{-1}
q_e	1.602×10^{-19} C

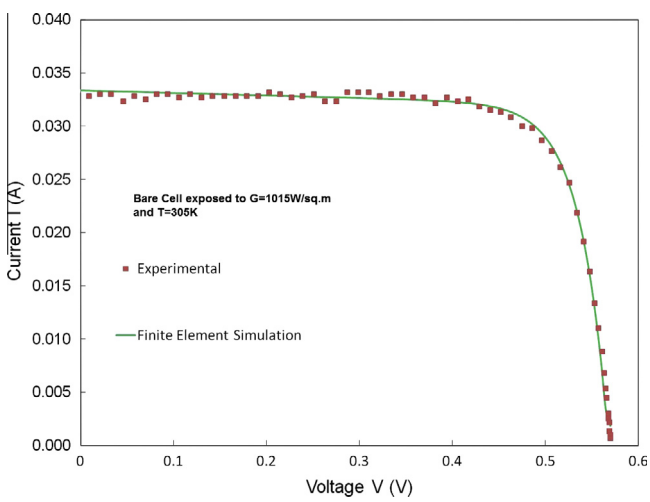

Fig. 15. Experimental and finite element simulated I–V characteristics of a solar cell under uniform illumination.

maximum illumination area of is 156 × 156 mm, with a nominal working distance of 200 mm. The uniformity of the illumination is 95%. In addition the setup included another small setup made of aluminium with a protractor scale that can be used to change the angles of the incident radiation on the CPV module. The IV characteristics of the system were recorded using an IV curve tracer from EKO instruments. The solar simulator was usually switched on for a warm up enabling a steady energy flux output. Using a temperature photodiode the simulator was calibrated while varying the current going to the xenon lamp.

While comparing the optical output considerable losses were found to occur due to such misalignments. The advantage of using the finite element modelling is that it can accurately help us in predicting the actual electrical output experienced under such conditions. Electrical analysis was carried out while projecting the optical power output on the misaligned solar cell. The characteristics obtained are plotted in Fig. 18 and compared with the experimental results obtained. An error of less than 1.5% can be seen between the modelled and the experimental results. It was important to implement the proper temperature while making this analysis, a temperature of 305 K and in the another 300 K was used as the cell temperature while making the analysis as observed during the experimentation process which is the primary reason for the slightly different V_{oc} values. Also important to incorporate was the losses occurring due to the absorption in the encapsulant which accounted for about 2%. This was obtained by experimentally checking the I–V characteristics of the solar cell with and without encapsulant as shown in Fig. 19.

4.3. Angular performance

The system was analysed at different angular positions to understand the overall energy production with variable sun positions. A special setup was utilised to change the angular position of the concentrator unit (Baig et al., 2013). The setup consisted of a base plate which may be inclined at any desired inclination with respect to the incoming illumination, in one dimension. The I–V characteristics were recorded at different angles using the solar simulator setup. Similarly, the unit concentrator with solar cell was analysed numerically using finite element method. The optical illumination output obtained from the concentrator is used as an input on the solar cell to analyse the electrical output.

The current density profile reflects the incoming illumination intensity over the solar cell. The regions receiving higher illumination intensities generate higher densities of current; the imbalance of current production along the solar cell surface tends to cause a local resistance in addition to the available series resistances of the solar cell. Moreover, it also causes a non uniform temperature across the surface of the solar cell. It has been shown by (Chemisana and Rosell, 2013) recently that the intensity profile along with temperature can both influence the electrical output of the system in both positive and negative manner. An improvement can be obtained in the electrical output by having a contrasting cooling arrangement for the solar cell. A good comparison may be seen in the magnitude of the current densities for different angles of incidence in Fig. 20. Current density in the fingers and busbars is not plotted in order to visualise the impact of the intensity profile and not for making a quantitative analysis. It can be clearly seen that the high flux incident on the cell in the case of non-uniform illumination causes non-uniform current generation along the cell. A peak may be noticed at the same place very clearly where there is high illumination. The current generated in the emitter due to the illumination flows through the adjacent fingers and then leads to the busbars, and finally gets absorbed.

Using the illumination intensity distribution obtained while carrying the optical analysis of the system, the

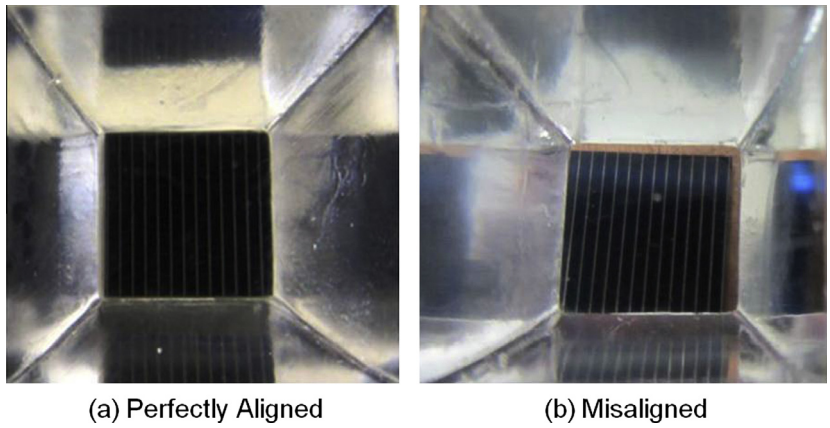

Fig. 16. Top view of the CPV system prepared using a copper back plate to visualise the misalignments.

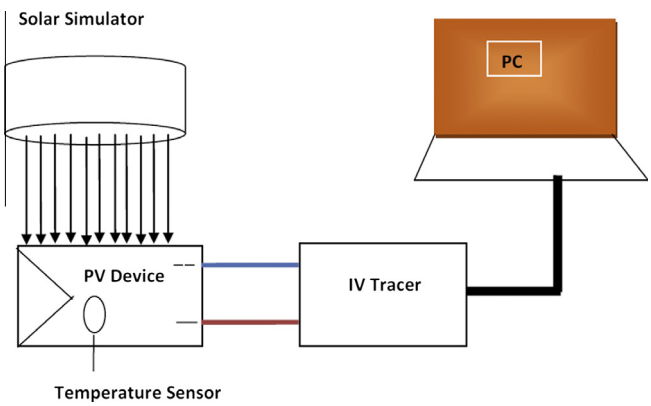

Fig. 17. Schematic of the setup used to carry out the experiments.

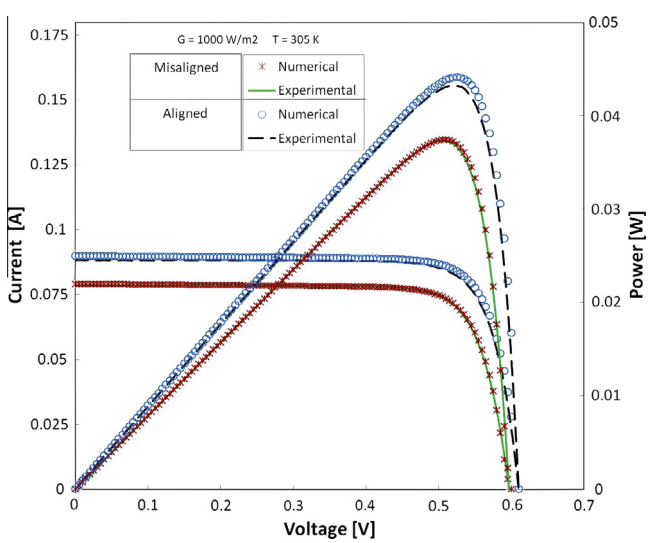

Fig. 18. *I–V* characteristics of a misaligned and properly aligned concentrator with solar cell.

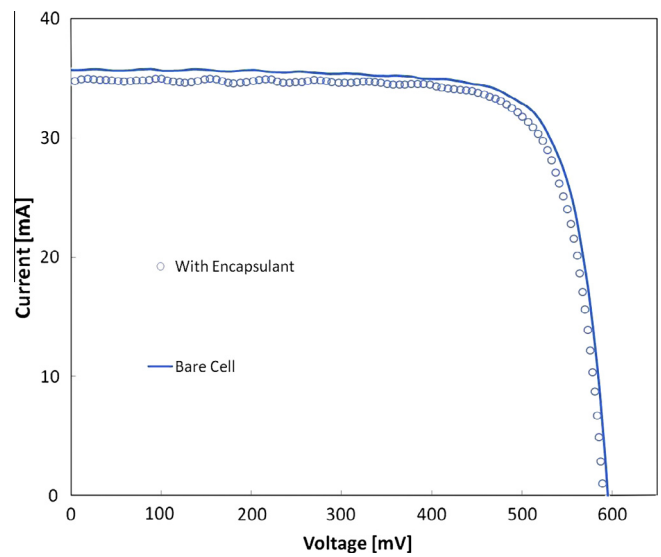

Fig. 19. Comparison of *I–V* characteristics of solar cell with and without encapsulant.

electrical analysis of the single concentrator unit is evaluated at different incident angles and compared with the experimental results. The summary of the results obtained is presented in Table 3.

The results obtained by using finite element method are found to be comparable with the results obtained by performing experiments. Slight deviations are found at incidence angles between 20° and 40° as shown in Fig. 21. Slightly higher fill factors are seen in the case of experimental results at these angles essentially due to the losses occurring at the edges of the concentrator due to the accumulation of encapsulation. The maximum power is obtained while the acceptance angle is 0°, with a value of 0.044 W and short circuit current of 90 mA at an incoming solar radiation of 1000 W/m^2.

The power ratio is defined as the ratio of the power output of the CPV unit and the bare cell. The power ratio is not same as the optical concentration ratio of the system it was evaluated for different angles and is presented under Fig. 22. The power ratio reveals the performance of the concentrator in a CPV unit in terms of the increase in the total power output. A maximum power ratio of 2.67 was found in our study when comparing the electrical output of the concentrator unit with the bare cell. The drop in

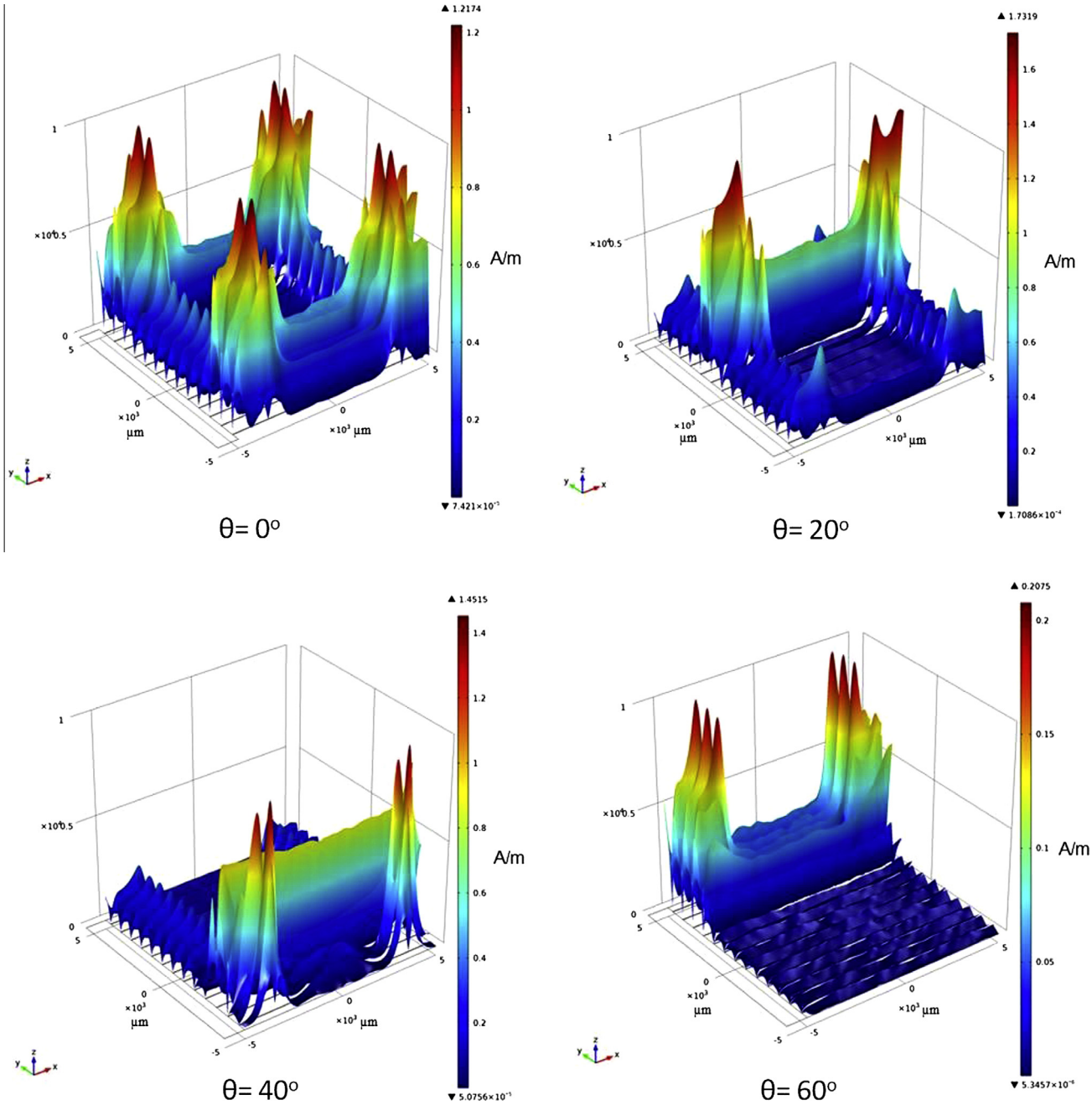

Fig. 20. Current density profiles on the emitter at different incident angles.

Table 3
Comparison of *I–V* characteristics obtained at different angular positions.

Numerical					Experimental			
θ_a (°)	P_{max} (W)	I_{sc} (mA)	V_{oc} (V)	*FF*	P_{max} (W)	I_{sc} (mA)	V_{oc} (V)	*FF*
0	0.044	90.00	0.610	0.804	0.043	88.35	0.610	0.802
10	0.043	88.02	0.610	0.803	0.043	87.94	0.608	0.804
20	0.041	84.11	0.610	0.800	0.039	78.80	0.604	0.819
30	0.037	76.65	0.605	0.802	0.032	65.81	0.598	0.816
40	0.028	59.32	0.600	0.793	0.023	49.27	0.585	0.794
50	0.007	16.51	0.550	0.761	0.006	12.99	0.546	0.799
60	0.003	8.13	0.550	0.675	0.004	9.29	0.524	0.758

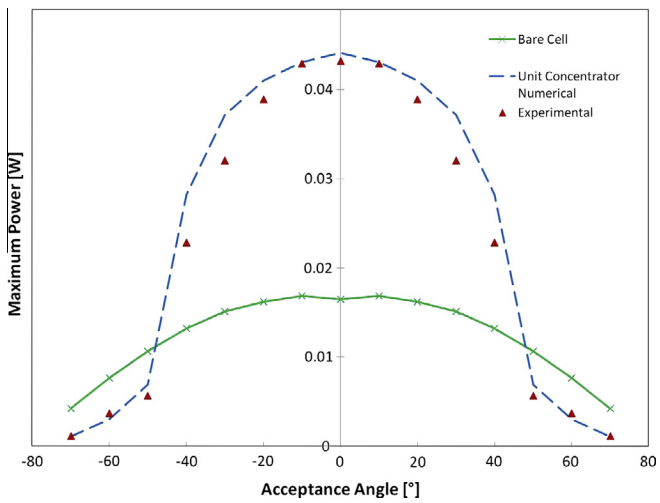

Fig. 21. Maximum power in a unit concentrator with varying incidence angles.

the power ratio of the unit for higher incidence angles may be due to the higher optical losses and the drop in the optical efficiency of the system.

4.4. Effect of non-uniformity

The non-uniform illumination distribution over the solar cell decreases the solar cell performance while comparing it under uniform illumination conditions. A detailed review over the causes and effects may be found under (Baig et al., 2012a,b). The refraction of light through the concentrator changes its intensity and spectrum considerably. In this study we analyse the impact of the change in the illumination intensity distribution under different angles of incidence neglecting the losses occurring by spectrum. A parametric analysis is carried out while biasing the cell to evaluate the *I–V* curve of the cells subjected to both uniform and non-uniform illumination patterns. Applying bias on the cell in small increments, the output power and current are modelled for both uniform and non-uniform illumination conditions. In both cases the total illumination on the cell is identical and the temperature is maintained as observed during the test conditions. Fig. 23 shows the simulated I_{sc} values under both uniform and non-uniform illumination conditions. A drop in the short circuit current can be observed due to the effect of non-uniformity having an average magnitude of 2.2%. A drop of about 0.5% is observed in the average cell efficiency due the non-uniformity of incoming flux distributions.

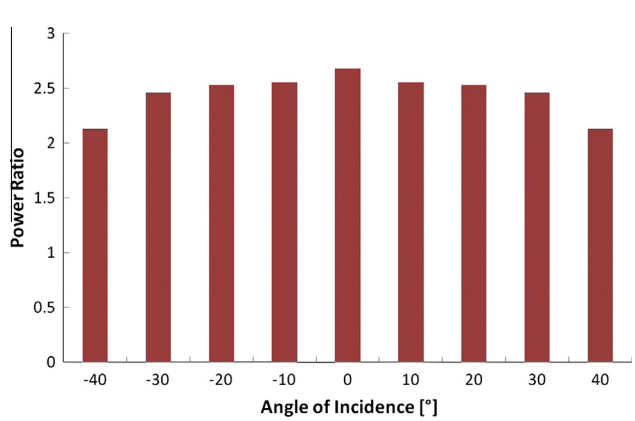

Fig. 22. Power ratio at different acceptance angles.

5. Thermal analysis

The solar cell temperature plays a key role in determining the overall energy produced by the solar cell, hence making it important to perform the thermal analysis of the overall system and determine the solar cell temperature. The temperature profile spread over the solar cell has also been shown to have a positive influence on the electrical output (Chemisana and Rosell, 2013). Determining the temperature distribution gives an idea if there is any need of cooling arrangement for the system. In the present study we analyse the operating temperature profile of the solar cell while performing a steady state heat transfer and then try to recalculate the electrical output of the solar cell. The thermal analysis is carried out using the finite element method, Fig. 24 shows the geometry of the system analysed. The most important step while solving the problem in finite element method is the meshing, which involves partitioning the geometry into smaller units known as the cells/mesh elements. These mesh elements can take different shapes and sizes. It is important that proper meshing be applied over the domain in order to obtain correct results. Different meshes were applied while carrying out the simulations and a grid independence test was carried out.

Typical heat transfer boundary conditions were applied to the system, a convective heat transfer condition was applied towards the top and the bottom surface of the system with $h = 10\ \mathrm{W/m^2\text{-}K}$ on the exterior surfaces of the system and a convective heat transfer coefficient of $h = 7\ \mathrm{W/m^2\text{-}K}$ on the interior surfaces. The source of heat transfer is considered to be the heat generated by the solar

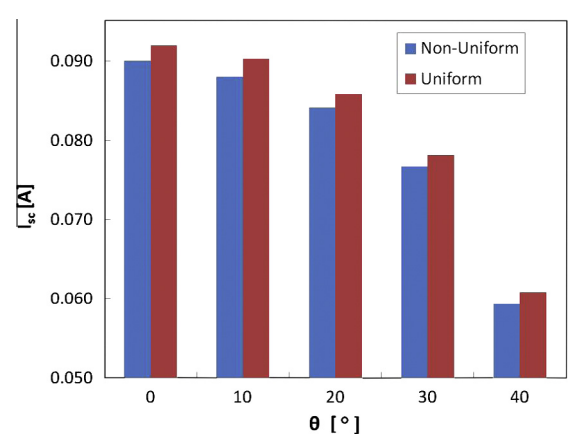

Fig. 23. Comparison of I_{sc} under uniform and non-uniform illumination conditions.

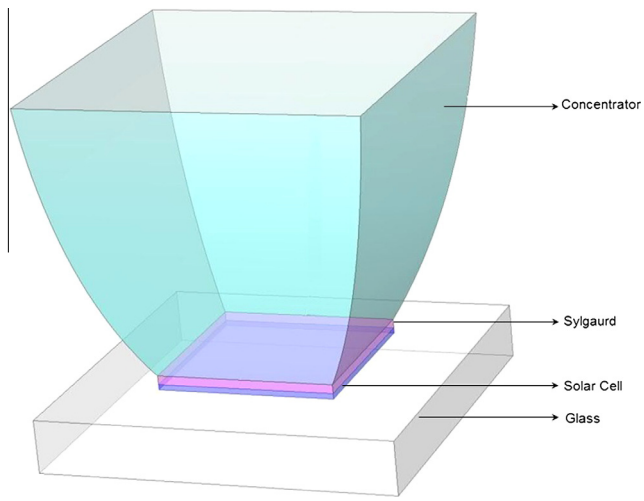

Fig. 24. Geometry used for the thermal analysis.

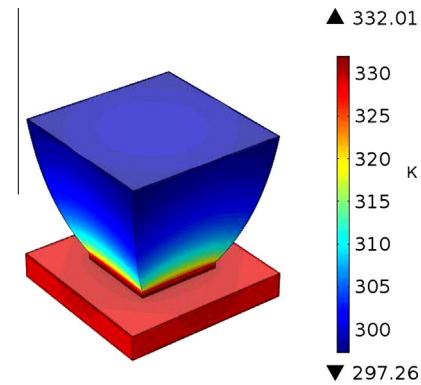

Fig. 25. Temperature distribution across the CPV system.

cell whilst converting the available irradiation to the electrical energy. Symmetry boundary conditions were applicable towards the side edges of the glass plate. The thermo-physical properties of the different materials used has been listed in Table 4 below.

A typical result obtained while simulating the system can be seen in Fig. 25, the temperature distribution varies in the range of 297–332 K in the system.

The thermal analysis is carried out for various angular positions, some of the results of which are presented in Fig. 26. It may be observed very well that the variation of the solar cell temperature is not that significant, however the temperature values are different at different angular positions. Starting with the highest temperature of 332 K in the case of the 0° incident angle, the temperature drops down to 299 K in the case of 60° incident angle. Also, important to note is that the temperature profile is in line with the incoming illumination flux intensity. Using the temperature distributions obtained from the thermal analysis, the T(x, y) is utilised to perform the electrical analysis is carried out for different angular positions to determine the steady state performance of the system.

6. System output

Using the temperature profiles obtained at different incident angles, the I–V characteristics are once again evaluated at the expected operating conditions to know what effect the temperature and its distribution has on the performance on the system. Fig. 27 shows the I–V characteristics of a unit concentrator under an illumination of 1000 W/m^2 at different incidence angles under test and expected operating conditions. It may be clearly seen that the temperature has a parasitic effect on the performance of the system. The V_{oc} of the concentrator unit drops significantly and so the maximum power point of the solar cell.

A cell temperature of 332 K was observed along the cell when the angle of incidence is 0°, which increasing angle of incidence the amount of illumination intensity falling over the solar cell decreases due to decreasing optical efficiency and so the operating temperature decreases to about 320 K at an angle of incidence of 40°. A considerable drop in the open circuit voltage and the maximum power occurs during this transformation which is detailed in Table 5. A considerable drop in fill factor amounting to an average of 4% is observed during actual operation of the CPV unit due to the temperature rise. About 14.6% of drop in the maximum power output and 11% drop in V_{oc} values can be observed. It may be noted that the V_{oc} values under test conditions drop with increasing angle of incidence, whereas they can be seen to increase during the operating conditions. This may be primarily attributed to the decreasing operating temperature with increasing angle of incidence under operating conditions.

7. Conclusions

A dielectric based 3DCCPC based PV unit was analysed for its optical, electrical and thermal performance. Extensive set of experimental and numerical results are presented to support its prospects as a Building integration system especially on tilted surfaces. It could be a good

Table 4
Thermo-physical properties of the different materials.

Component	Solar cell	Concentrator	Glass plate	Encapsulation
Material	Silicon	Polyurethane	Glass	Sylguard
Thickness (mm)	0.3	14.5	3	0.5
Density (kg m^{-3})	2329	1162	2500	1030
Thermal conductivity (W m^{-1} K^{-1})	149	0.1875	1.4	0.16
Heat capacity (J mol^{-1} K^{-1})	19.789	1465	750	1030

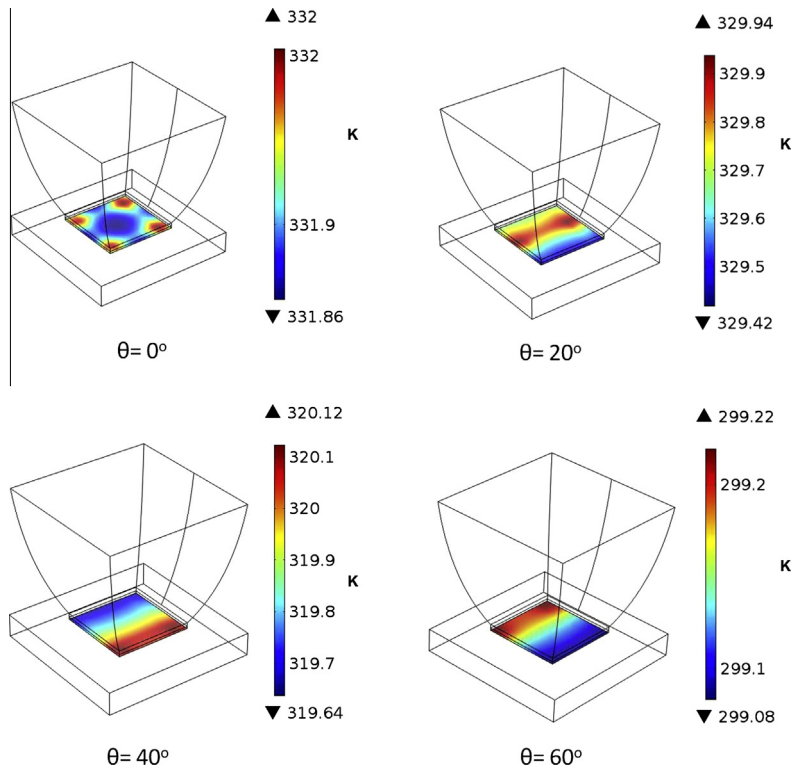

Fig. 26. Temperature contours on the concentrator and the solar cells.

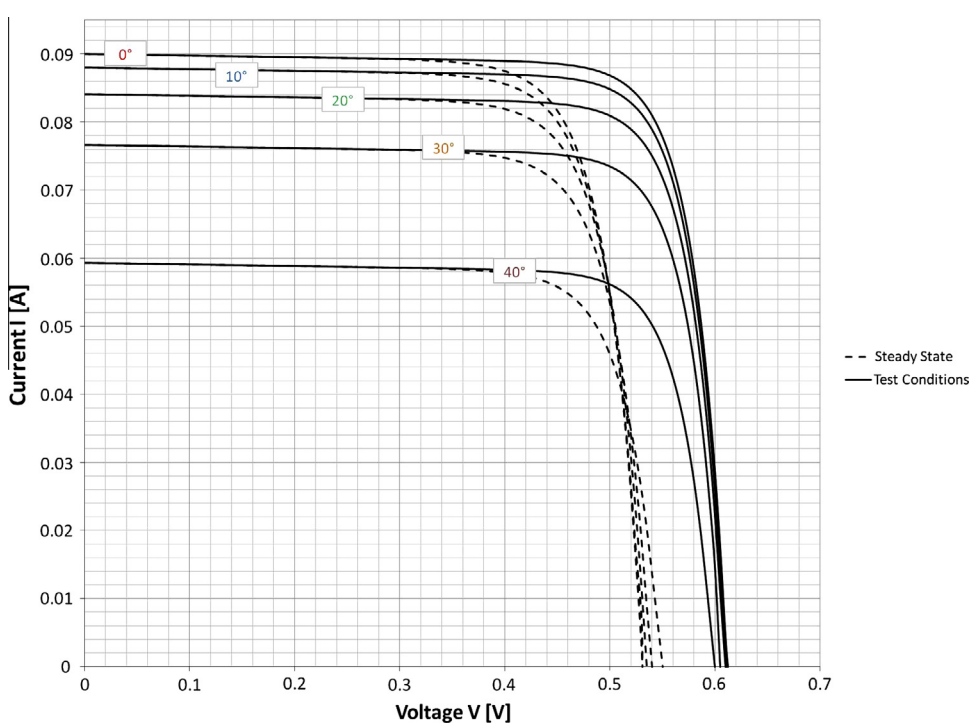

Fig. 27. *I–V* characteristics at different incident angles under test and steady state conditions.

application titled façade, sky lighting or a roof application. Using the flux distribution obtained while performing the optical analysis the electrical modelling of the solar cell was performed using finite element method. The *I–V* characteristics of the system under different incidence angles was analysed and compared with experimental results. It

Table 5
Comparison of the electrical characteristics of the solar cell under test and operating conditions.

Angle of incidence	Test conditions			Operating conditions		
	V_{oc}	Pm	FF	V_{oc}	Pm	FF
0	0.612	0.044	0.802	0.531	0.037	0.770
10	0.611	0.043	0.802	0.535	0.036	0.766
20	0.610	0.041	0.800	0.540	0.035	0.764
30	0.605	0.037	0.802	0.545	0.032	0.765
40	0.600	0.028	0.793	0.550	0.025	0.773

was shown how misalignments can cause a drop in the overall performance and minimisation of such errors is to be avoided during the manufacture of the system. The impact of non-uniformity of flux distribution showed an average drop of 2.2% in the I_{sc} values, which would again reflect the same in the solar cell efficiency. The electrical efficiency of the system was used to calculate the heat dissipated by the solar cell to the rest of the unit. Further the temperature of the solar cell and its profile is used to analyse the steady state operation of the solar cell under operating conditions. The temperature was found to have a parasitic effect on the overall performance of the system bringing about 14.6% drop in the overall power production. The average fill factor was found to drop from 0.8 to 0.76 during different incident angles. Future work on the system would be to test it under outdoor conditions and perform accelerated experiments to understand the life cycle of the system.

References

Anon, 2008. Information about Dow Corning Brand Silicone Encapsulants, Dow Corning, Midland, USA.

Anon, 2009. Datasheet: ABET sun2000 class-A, ABET Technologies Inc., Milford, USA.

Baig, H., Heasman, K.C., Sarmah, N., Mallick, T.K., 2012. Solar cells design for low and medium concentrating photovoltaic systems. In: 8th International Conference on Concentrating Photovoltaic Systems, Toledo, Spain.

Baig, H., Heasman, K.C., Mallick, T.K., 2012b. Non-uniform illumination in concentrating solar cells. Renew. Sustain. Energy Rev. 16, 5890–5909.

Baig, H., Sarmah, N., Heasman, K.C., Mallick, T.K., 2013. Numerical modelling and experimental validation of a low concentrating photovoltaic system. Sol. Energy Mater. Solar Cells 113, 201–219.

Biancardo, M., Taira, K., Kogo, N., Kikuchi, H., Kumagai, N., Kuratani, N., Inagawa, I., Imoto, S., Nakata, J., 2007. Characterization of microspherical semi-transparent solar cells and modules. Sol. Energy 81, 711–716.

Chemisana, D., 2011. Building integrated concentrating photovoltaics: a review. Renew. Sustain. Energy Rev. 15 (1), 603–611.

Chemisana, D., Rosell, J.I., 2013. Electrical performance increase of concentrator solar cells under Gaussian temperature profiles. Progr Photovolt: Res Appl, 444–455.

<http://www.smooth-on.com/tb/files/CRYSTAL_CLEAR_200_TB.pdf>.

Hughes, E., 2009. Global Energy Network Institute, Suntech to Develop 20% of BIPV Solar Rooftop Program Projects. In: <PV-tech.org>, <http://www.geni.org/globalenergy/library/technical-articles/generation/solar/pv-tech.org/suntech-to-develope-20%25-of-bivp-solar-rooftop-program-projects,-china/index.shtml>.

Heasman, K.C., Roberts, S., Brown, M., Baistow, I., Devenport, S., Bruton, T.M., 2007. Development of LGBC solar cells for use at concentration factors up to 100×. In: 4th International Conference on Solar Concentrators (ICSC-4), Spain.

Lausten, J., 2008. Energy efficiency requirements in building codes, energy efficiency policies for new buildings, IEA, pp. 7.

Lu, Z.H., Song, Q., Li, S.Q., Yao, Q., Othman, A., 2009. The effect of non-uniform illumination on the performance of conventional polycrystalline silicon solar cell. In: Goswami, D.Y., Zhao, Y. (Eds.), . In: Proceedings of ISES World Congress 2007, vol. I–V. Springer, Berlin Heidelberg, pp. 1445–1448.

Magazine, S.T., 2010. The curved solar power rooftop tile, homeowners now have better looking options <http://www.solarthermalmagazine.com/2010/10/23/the-curved-solar-power-rooftop-tile-homeowners-now-have-better-looking-options/>.

Mammo, E.D., Sellami, N., Mallick, T.K., 2013. Performance analysis of a reflective 3D crossed compound parabolic concentrating photovoltaic system for building façade integration. Progr Photovolt: Res Appl, 1095–1103.

Nilsson, J., Håkansson, H., Karlsson, B., 2007. Electrical and thermal characterization of a PV-CPC hybrid. Sol. Energy 81, 917–928.

O'Gallagher, J.J., 2008. Nonimaging Optics in Solar Energy. Morgan & Claypool Publishers, San Rafael, Calif..

Park, K.E., Kang, G.H., Kim, H.I., Yu, G.J., Kim, J.T., 2010. Analysis of thermal and electrical performance of semi-transparent photovoltaic (PV) module. Energy 35, 2681–2687.

Petter Jelle, B., Breivik, C., Drolsum Røkenes, H., 2012. Building integrated photovoltaic products: a state-of-the-art review and future research opportunities. Sol. Energy Mater. Sol. Cells 100, 69–96.

Rosell, J.I., Ibáñez, M., 2006. Modelling power output in photovoltaic modules for outdoor operating conditions. Energy Conv. Manage. 47 (15–16), 2424–2430.

Sarmah, N., Richards, B.S., Mallick, T.K., 2011. Evaluation and optimization of the optical performance of low-concentrating dielectric compound parabolic concentrator using ray-tracing methods. Appl. Opt. 50, 3303–3310.

Sellami, N., Mallick, T.K., 2012. Design of Nonimaging static solar concentrator for window integrated photovoltaic. In: 8th International Conference on Concentrating Photovoltaic Systems, Toledo, Spain.

Sellami, N., Mallick, T.K., 2013. Optical efficiency study of PV crossed compound parabolic concentrator. Appl Energy 102, 868–876.

Sellami, N., Mallick, T.K., McNeil, D.A., 2011. Optical characterisation of 3-D static solar concentrator. In: International Renewable Energy Congress: IREC2011, Hammamet, Tunisia. pp. 321–326.

Sellami, N., Ghosh, A., Mallick, T.K., 2011. Comparative experimental characterisation of reflective and refractive type 3-d static low concentrating photovoltaic system. In: 7th Photovoltaic Science Applications and Technology, pp. 245–248.

Sellami, N., Mammo, E.D., Mallick, T.K., 2011. Experimental characterisation of reflective and refractive type 3-D static low concentrating photovoltaic system. In: Photovoltaic Science and Technology Conference, Edinburgh, UK.

Tripanagnostopoulos, Y., Siabekou, C., Tonui, J.K., 2007. The Fresnel lens concept for solar control of buildings. Sol. Energy 81, 661–675.

Tripanagnostopoulos, Y., Georgostathis, P., Iliopoulou, A., 2009. Optical study of new designs for CPVT systems. In: Concentrating Photovoltaics Optics and Power, Darmstadt, Germany.

Yamada, N., Kanno, K., Hayashi, K., Tokimitsu, T., 2011. Performance of see-through prism CPV module for window integrated photovoltaics. Opt. Exp. 19, A649–A656.

Yoon, J.-H., Song, J., Lee, S.-J., 2011. Practical application of building integrated photovoltaic (BIPV) system using transparent amorphous silicon thin-film PV module. Sol. Energy 85, 723–733.

Zacharopoulos, A., Eames, P.C., McLarnon, D., Norton, B., 2000. Linear dielectric non-imaging concentrating covers for PV integrated building facades. Sol. Energy 68, 439–452.